Ки&М

MODELS IN PHYSICS AND TECHNOLOGY

UDC: 519.6

Nonlinear modeling of oscillatory viscoelastic fluid with variable viscosity: a comparative analysis of dual solutions

P. Vaidehi, J. Sasikumar[a]

Department of Mathematics, Faculty of Engineering and Technology, SRM Institute of Science and Technology, Kattankulathur, Tamil Nadu, 603203, India

Corresponding author E-mail: [a] sasikumj@srmist.edu.in

The viscoelastic fluid flow model across a porous medium has captivated the interest of many contemporary researchers due to its industrial and technical uses, such as food processing, paper and textile coating, packed bed reactors, the cooling effect of transpiration and the dispersion of pollutants through aquifers. This article focuses on the influence of variable viscosity and viscoelasticity on the magnetohydrodynamic oscillatory flow of second-order fluid through thermally radiating wavy walls. A mathematical model for this fluid flow, including governing equations and boundary conditions, is developed using the usual Boussinesq approximation. The governing equations are transformed into a system of nonlinear ordinary differential equations using non-similarity transformations. The numerical results obtained by applying finite-difference code based on the Lobatto IIIa formula generated by bvp4c solver are compared to the semi-analytical solutions for the velocity, temperature and concentration profiles obtained using the homotopy perturbation method (HPM). The effect of flow parameters on velocity, temperature, concentration profiles, skin friction coefficient, heat and mass transfer rate, and skin friction coefficient is examined and illustrated graphically. The physical parameters governing the fluid flow profoundly affected the resultant flow profiles except in a few cases. By using the slope linear regression method, the importance of considering the viscosity variation parameter and its interaction with the Lorentz force in determining the velocity behavior of the viscoelastic fluid model is highlighted. The percentage increase in the velocity profile of the viscoelastic model has been calculated for different ranges of viscosity variation parameters. Finally, the results are validated numerically for the skin friction coefficient and Nusselt number profiles.

Keywords: viscoelastic fluid model, variable viscosity, Lorentz force, porous channel, oscillatory flow, HPM, heat transfer

1. Introduction

In the past few years, there has been a growing interest in studying non-Newtonian magnetohydrodynamic (MHD) flows using various geometrical models. The industrial and technical applications of viscoelastic fluid flow across porous media have attracted the attention of contemporary researchers. These applications include food processing, paper and textile coating, packed bed reactors, etc. Bataller has focused on the study of an incompressible uniform second-grade fluid flowing over a non-isothermal stretching sheet with nonuniform internal heat generation/absorption and investigated the effects of various factors such as internal heat generation/absorption, viscous dissipation, thermal radiation and work due to deformation [Bataller, 2007]. Falade et al. investigated the impact of suction or injection on the unsteady oscillatory flow in a vertical channel with nonuniform wall temperature. The study [Falade et al., 2017] also considered the presence of a transverse magnetic field, accounting for velocity slip at the lower plate and suggested a significant influence of injection on the flow behavior and frictional forces within the system. By extending the study to irregular channels and considering the behavior of a non-Newtonian fluid, [Venkateswarlu et al., 2019] contributed to a more comprehensive understanding of fluid dynamics in complex geometries. The findings obtained from the analytical solutions and the graphical analysis presented the influence of various flow parameters on the fluid flow characteristics in an asymmetric wavy channel. Raptis analyzed the steady flow of an elastico-viscous fluid with radiation and suggested insights into the heat transfer characteristics of such a system. The numerical solution for the temperature field allows for a visual representation of the temperature profiles, providing a better understanding of the behavior of the fluid under given conditions [Raptis, 1999]. The impact of slip velocity at the wall on the flow and mass transfer characteristics of an electrically conducting viscoelastic fluid presented specifically using Walters' liquid B model. The study focuses on a scenario where the fluid flows past a stretching sheet embedded in a porous medium. Furthermore, the investigation [Mahmoud, 2010] considers the presence of chemical reactions and concentration-dependent viscosity.

A novel approach is adopted by [Sasikumar, Senthamarai, 2022], which involves modeling the geometric shape of the blood vessels and veins as tapered curvy walls with varying cross-sections. This approach offers advantages compared to other geometrical channel shapes commonly used in similar studies. The blood is characterized as a viscoelastic fluid and an optically thick fluid that flows through porous structures, such as blood tissues. The impact of a slip parameter on hydro-magnetic oscillatory flow coupled with heat and mass transfer in an asymmetric wavy channel filled with a species concentration through a porous medium is discussed by [Sasikumar, Govindarajan, 2016]. The study conducted by [Rundora, Makinde, 2013] discusses the investigation of the thermal effects of the suction/injection Reynolds number and other flow parameters on an unsteady reactive temperature-dependent viscosity third-grade fluid in a porous channel filled with a saturated porous medium. Mukhopadhyay et al. analyzed a viscous incompressible fluid with varying viscosity by considering free convective flow and radiative heat transfer over a stretched porous vertical plate. The system under investigation [Mukhopadhyay, Layek, 2008] exhibits invariance due to specific relationships among the parameters of the scaling group of transformations. The influence of heat transfer on the MHD oscillatory flow of a Jeffrey fluid with a variable viscosity model through a porous medium has been explored by Al-Khafajy. The investigation [Al-Khafajy, 2016] focuses on understanding the influence of several emerging parameters on the velocity field and temperature field of the fluid. The oscillatory flow of an elastico-viscous conducting fluid across a moving plate with changing suction has been studied by [Baag et al., 2022] in a porous medium. The study incorporates the Darcy model to account for the resistive force exerted by the permeability of the medium in the momentum equation. Sasikumar et al. analyzed the influence of suction and injection on the unsteady oscillatory flow of an incompressible viscous electrically conducting fluid within an asymmetric channel filled within a porous medium [Sasikumar, Bhati, Bhaskar, 2020].

The magnetohydrodynamic (MHD) oscillatory flow of a viscous fluid in an asymmetric channel with a permeable structure and a heat source has been studied in [Sasikumar, Harinisha, Anitha, 2019]. The governing equations are considered under typical MHD flow assumptions and exact solutions are obtained for pressure, momentum, and temperature profiles. A theoretical study that aims to investigate the effect of controlling parameters on velocity, temperature, and temperature gradient in the boundary layer of a Casson fluid with variable viscosity and thermal conductivity has been conducted by [Animasaun, 2015a]. The study focuses on a vertical surface embedded in a stratified medium with suction and exponentially decaying space-dependent internal heat generation. An incompressible electrically conducting Casson fluid flows through a vertical porous plate, and [Animasaun, 2015b] examined the influence of various factors on these flow properties. The study considers thermophoresis, the Dufour effect, temperature-dependent thermal conductivity and viscosity, viscous dissipation, nth-order chemical reaction, and suction. The novelty of the study is addressed by [Mishra, Dash, Acharya, 2013] by examining the influence of time-dependent fluctuating suction and permeability on the behavior of viscoelastic fluids, which is relevant due to the viscoelastic nature exhibited by many industrial fluids. Selvi et al. delved into the investigation of unsteady MHD convective flow in a vertical porous channel, taking into account various factors such as viscous dissipation, non-Newtonian behavior of the fluid (Jeffrey fluid), diffusion-thermo effects, thermal diffusion, and suction [Selvi, Muthuraj, 2018]. The inclusion of a comparison between the HAM solution and numerical solutions obtained through ND Solver in Mathematica adds credibility to the findings, ensuring the accuracy and reliability of the proposed method.

The influence of variable viscosity on periodic Darcy flow within a vertical channel, incorporating suction/injection, slip boundary conditions, and using Casson fluid as a non-Newtonian model is studied by [Abbas et al., 2020]. It highlights the specific behavior of non-Newtonian fluids and the impact of TDV on their flow characteristics. The investigation of radiation and mass transfer effects on MHD oscillatory flow of a Jeffery fluid through a porous channel in the presence of chemical reaction is conducted by [Al-Khafajy, 2019]. Incorporating the variable viscosity assumption, where viscosity is modeled as an exponential function of temperature, adds complexity to the analysis. Ali investigated how temperature-dependent viscosity affected heat transfer and laminar mixed convection boundary layer flow on a constantly moving vertical surface. The article [Ali, 2006] thoroughly analyzed the subject, highlighting the intricate relationships between variable viscosity and mixed convection boundary layer flow. Salem addressed the problem of flow and heat transfer for an electrically conducting viscoelastic fluid over a continuously stretching sheet in the presence of a uniform magnetic field. The inclusion of power-law variation in the sheet temperature and the consideration of temperature-dependent fluid viscosity and thermal conductivity add complexity to the analysis [Salem, 2007]. Pearson offers valuable insights into the behavior of viscous fluids with temperature-dependent viscosity in a plane channel, studied by the presence of a thin thermal boundary layer at each wall, with an even thinner shear layer detached from the wall and embedded within the thermal boundary layer. The dimensionless formulation and identification of key dimensionless groups enhance the clarity of the analysis [Pearson, 1977]. Raju et al. delved into an analytical investigation of the unsteady MHD free convective flow of an electrically conducting Jeffery fluid past an infinite vertical porous flat plate. The consideration of the slip flow regime and the application of a uniform magnetic field perpendicular to the plate further enrich the study [Raju et al., 2018].

An analytical technique for solving nonlinear problems, utilizing a combination of homotopy in topology and the Maclaurin series has been discovered in [Liao, 1995]. The method is introduced using a simple nonlinear equation, showcasing its potential application in various nonlinear problems. Sasikumar et al. explored the impact of suction or injection on the unsteady oscillatory flow of an incompressible, viscous, electrically conducting fluid through a channel filled with a porous medium [Sasikumar, Bhuvaneshwari, Govindarajan, 2018]. The channel has a nonuniform wall

temperature, and a uniform magnetic field is applied perpendicular to the channel. The role of Brownian motion in fluid dynamics, addressing both theoretical and empirical aspects has been examined in [Animasaun et al., 2019]. The significance of this analysis lies not only in the field of mathematical physics but also in the context of statistical techniques and their application to fluid flow research. Ogulu et al. presented a mathematical investigation into blood flow during deep heat muscle treatment. By considering blood vessels as long tubes with slowly varying radii, the study [Ogulu, Bestman, 1993] aimed at the underlying mechanisms behind the therapeutic effects of hot baths for cuts and ice packs for bruises. The behavior of Casson fluid in a wavy channel under the influence of velocity slip and heat transfer effects has been analyzed in [Vaidehi, Sasikumar, 2023a]. The combination of analytical and numerical approaches enhanced the understanding of the system dynamics and discussed the non-Newtonian fluid behavior and its implications for heat transfer in complex flow systems. Vaidehi et al. studied the effect of thermo-diffusion on the behaviour of viscoelastic fluid in an asymmetric wavy channel under the influence of an external magnetic field and heat source. The results of this investigation [Vaidehi, Sasikumar, 2023b] can be applied in industrial applications using viscoelastic fluids, offering insights for process optimization and design considerations.

Jiang et al. addressed the unsteady MHD flow of a generalized second grade fluid through a porous medium, considering the impact of Hall effects on heat and mass transfer. The study [Jiang, Zhang, Wang, 2020] incorporates a fractional derivative in the constitutive equation, employing the second grade fluid model. The effects of radiation and Hall current on the unsteady (MHD) free convective flow in a vertical channel filled with a porous medium has been discussed by [VeeraKrishna, Subba Reddy, Chamkha, 2018]. Using the Laplace transform approach, [Siva et al., 2020] presented a theoretical analysis of the transient rotating electro-osmotic flow of couple stress fluid in a microchannel. Barkilean et al. presented an in-depth investigation into the realm of nanofluids, an area of research that has garnered considerable attention for its potential to significantly enhance heat transfer efficiency when compared to conventional base fluids [Barkilean, Jagadeesan, 2023]. A numerical investigation of unsteady mixed convection in an open, partially porous horizontal channel with an internal heat-generating source has been presented in [Astanina, Sheremet, 2019]. The channel features adiabatic outer walls and contains a Newtonian heat-conducting fluid with temperature-dependent viscosity. The time-dependent natural convection heat transfer in a closed square cavity containing a non-Newtonian fluid, with an isothermal energy source located on the lower wall, has been proposed by [Loenko, Sheremet, 2020]. A mathematical model for investigating the nonlinear hydro-elastic response of a narrow channel wall connected to a spring with cubic nonlinearity, interacting with a pulsating viscous liquid filling the channel has been analyzed by [Popov, Popova, 2022]. There is still more research to be done on the complex dynamics of viscoelastic fluid flow over porous media and how it relates to time-dependent viscosity and viscoelasticity. A strong basis for further research and developments in this area is provided by the mathematical model and numerical approaches used. The outcomes of this novel research contribute to a deeper understanding of fluid flow phenomena, which can be leveraged to optimize industrial processes, such as food processing, paper and textile coating, packed bed reactors, and the dispersion of pollutants through aquifers.

The present study undertakes the following investigations based on the aforementioned survey.

a) How does the rate of increase/decrease in the skin friction coefficient at thermal radiation parameter N compare to the variations observed in the viscoelasticity of the second-order fluid?

b) How do the viscosity variation parameter and the Lorentz force interact with each other in determining the velocity behavior of the viscoelastic fluid?

c) How does the variation in the Peclet number influence the fluid temperature distribution across the channel?

2. Mathematical model and derivation

An unsteady, incompressible laminar fluid flow of a viscoelastic fluid via thermally radiating wavy walls is considered. The following model, in which x passes through the middle of the channel and the y-direction is normal to the x-direction, is used to depict the physical configuration (see Fig. 1 of the flow). It is assumed that the fluid flow is normal to the strength of the constant magnetic field B_0. Since the magnetic Reynolds number is substantially lower than the external one, it is presumed that the generated magnetic fields are insignificant. As [Raju et al., 2018] proposed, some terms (viscous dissipation and Joule heating) are omitted as modest velocities typically present in periodic and free convection flows. The equations governing the flow, heat and mass transport of a viscous incompressible fluid can be expressed as follows under the aforementioned assumptions and using the Boussinesq approximation [Venkateswarlu et al., 2019].
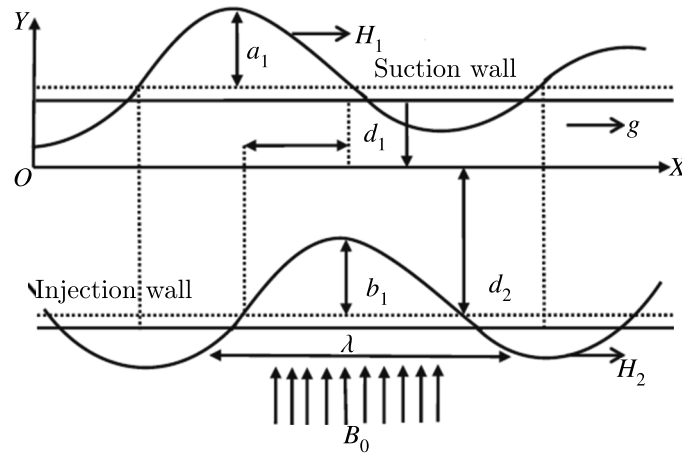

Figure 1. Physical configuration

The equations describing the walls of an asymmetric wavy channel are given by [Venkateswarlu et al., 2019]

$$H_1 = d_1 + a_1 \cos\left(\frac{2\pi}{\lambda'}(x)\right),$$

$$H_2 = -d_2 - b_1 \cos\left(\frac{2\pi}{\lambda'}(x) + \psi\right),$$
(1)

where a_1, b_1, d_1, d_2 and ψ satisfy the condition $a_1^2 + b_1^2 + 2a_1b_1 \cos\psi \leqslant (d_1 + d_2)^2$,

$$\rho\left(\frac{\partial u}{\partial t} - v_0\frac{\partial u}{\partial y}\right) = -\frac{\partial p}{\partial x} + \frac{\partial}{\partial y}\left(\mu(T)\left(\frac{\partial u}{\partial y}\right)\right) + \beta\frac{\partial^3 u}{\partial y^2 \partial t} - \left(\frac{\mu(T)}{k^*} - \sigma B_0^2\right)u + \rho g\beta_T(T - T_0) + \rho g\beta_C(C - C_0),$$
(2)

$$\rho C_p\left(\frac{\partial T}{\partial t} - v_0\frac{\partial T}{\partial y}\right) = K\frac{\partial^2 T}{\partial y^2} - \frac{\partial q}{\partial y} + Q_H(T - T_0),$$
(3)

$$\frac{\partial C}{\partial t} - v_0\frac{\partial C}{\partial y} = D\frac{\partial^2 C}{\partial y^2} - Kr^*(C - C_0),$$
(4)

$$u = 0, \quad T = T_0 + (T_1 - T_0)e^{i\omega t} \quad \text{and} \quad C = C_0 + (C_1 - C_0)e^{i\omega t} \quad \text{on } y = H_1,$$
(5)

$$u = 0, \quad T = T_0 \quad \text{and} \quad C = C_0 \quad \text{on } y = H_2.$$
(6)

The heat flow due to radiation using Plank's approximation is given as [Ogulu, Bestman, 1993]

$$\frac{\partial q}{\partial y} = 4\alpha^2(T - T_0).$$
(7)

Variables with no dimensions are given by

$$\overline{x} = \frac{x}{\lambda'}, \quad \overline{y} = \frac{y}{d}, \quad \overline{u} = \frac{u}{U}, \quad h_1 = \frac{H_1}{d_1}, \quad h_2 = \frac{H_2}{d_2}, \quad \overline{t} = \frac{tU}{d}, \quad d = \frac{d_2}{d_1},$$

$$a = \frac{a_1}{d_1}, \quad b = \frac{b_1}{d_1}, \quad S = \frac{v_0 d}{\mu}, \quad \overline{p} = \frac{pd^2}{\rho\mu\lambda'U}, \quad Da = \frac{k^*}{d^2}, \quad Re = \frac{Ud}{\mu}, \quad Sc = \frac{D}{Ud},$$

$$Gr = \frac{g\beta_T d^2(T_1 - T_0)}{\mu U}, \quad Gc = \frac{g\beta_C d^2(C_1 - C_0)}{\mu U}, \quad Pe = \frac{Ud\rho C_p}{K}, \quad Q = \frac{Q_H d^2}{K},$$

$$\theta = \frac{T - T_0}{T_1 - T_0}, \quad \phi = \frac{C - C_0}{C_1 - C_0}, \quad N = \frac{4\alpha^2 d^2}{K}, \quad Ha = \frac{B_0^2 \sigma d^2}{\rho\mu}, \quad Kr = \frac{dKr^*}{U}. \tag{8}$$

The dimensionless governing equations, together with the necessary boundary conditions, are given by

$$Re\left(\frac{\partial u}{\partial t} - S\frac{\partial u}{\partial y}\right) = -\frac{\partial p}{\partial x} + \frac{\partial}{\partial y}\left(\mu(\theta)\left(\frac{\partial u}{\partial y}\right)\right) + \beta\frac{\partial^3 u}{\partial y^2 \partial t} + Gr\theta + Gc\phi - \left(Ha - \frac{\mu(\theta)}{Da}\right)u, \tag{9}$$

$$Pe\left(\frac{\partial\theta}{\partial t} - S\frac{\partial\theta}{\partial y}\right) = \frac{\partial^2\theta}{\partial y^2} + (N + Q)\theta, \tag{10}$$

$$\frac{\partial\phi}{\partial t} - S\frac{\partial\phi}{\partial y} = Sc\frac{\partial^2\phi}{\partial y^2} - Kr\phi, \tag{11}$$

$$u = 0, \quad \theta = e^{i\omega t} \quad \text{and} \quad \phi = e^{i\omega t} \quad \text{on } y = h_1, \tag{12}$$

$$u = 0, \quad \theta = 0 \quad \text{and} \quad \phi = 0 \quad \text{on } y = h_2, \tag{13}$$

$$h_1 = 1 + a\cos(2\pi x),$$
$$h_2 = -d - b\cos(2\pi x + \psi), \tag{14}$$

where $\mu(\theta) = \frac{\mu(T)}{\mu_0}$. There are several mathematical models in the literature that explain the phenomenon of variable viscosity. Here, the influence of temperature on viscosity variations is analyzed using the Reynolds viscosity model, as suggested by [Abbas et al., 2020],

$$\mu(\theta) = e^{-\epsilon\theta}. \tag{15}$$

Reducing equation (15) by using Maclaurin's series, we obtain

$$\mu(\theta) = 1 - \epsilon\theta + \frac{1}{2}(\epsilon\theta)^2, \tag{16}$$

where ϵ represents the viscosity variation parameter and θ is the dimensionless temperature.

3. Method of solution

After solving the system of partial differential equations (9)–(11), the associated solutions can be reduced to a nondimensional system of ordinary differential equations using the method of separation of variables. The equations for pressure gradient, velocity, temperature and concentration for purely oscillatory flow are as follows:

$$-\frac{dP}{dx} = \lambda e^{i\omega t},$$
$$u(y, t) = u_0(y)e^{i\omega t},$$
$$\theta(y, t) = \theta_0(y)e^{i\omega t},$$
$$\phi(y, t) = \phi_0(y)e^{i\omega t}. \tag{17}$$

The following ordinary differential equations are obtained by applying (17) to equation (9)–(13) and replacing u, θ and ϕ:

$$\left(\mu(\theta) + \beta i\omega\right)u_0'' + \left(S + \frac{\partial}{\partial y}(\mu(\theta))\right)u_0' - \left(\frac{\mu(\theta)}{Da} + Ha + Rei\omega\right)u_0 + \lambda + Gr\theta_0 + Gc\phi_0 = 0, \quad (18)$$

$$\theta_0'' + S\theta_0' + (N + Q - Pei\omega)\theta_0 = 0, \quad (19)$$

$$\phi_0'' + \frac{S}{Sc}\phi_0' - \frac{Kr + i\omega}{Sc}\phi_0 = 0. \quad (20)$$

Equations (18)–(20) are subjected to the following boundary conditions:

$$u_0 = 0, \quad \theta_0 = 1 \quad \text{and} \quad \phi_0 = 1 \quad \text{on } y = h_1, \quad (21)$$

$$u_0 = 0, \quad \theta_0 = 0 \quad \text{and} \quad \phi_0 = 0 \quad \text{on } y = h_2. \quad (22)$$

Substituting equation (16) into (18), the momentum equation is formulated as

$$\left(1 - \epsilon\theta_0 + \frac{1}{2}(\epsilon\theta_0)^2 + \beta i\omega\right)u_0'' + \left(S - \epsilon\theta_0' + \epsilon^2\theta_0\theta_0'\right)u_0' - \left(\frac{1 - \epsilon\theta_0 + \frac{1}{2}(\epsilon\theta_0)^2}{Da} + Ha + Rei\omega\right)u_0 +$$
$$+ \lambda + Gr\theta_0 + Gc\phi_0 = 0. \quad (23)$$

3.1. Basic idea on the homotopy perturbation method (HPM)

In the present study, the momentum equation is nonlinear. Obtaining a closed-form solution to the model is a challenging task. For these kinds of problems, several approximate solution techniques have been developed, including perturbation methods, numerical solutions, and others. One such approximate technique which [Liao, 1995] proposed is the homotopy perturbation method (HPM). The method is simple, effective, and convenient for solving nonlinear and coupled boundary value problems. The homotopy perturbation technique (HPM), which combines the perturbation method and the homotopy method, keeps all of the benefits of conventional perturbation methods while eliminating their disadvantages, such as the limitation of small parameters that characterize the regular perturbation. [Liao, 1995] presented the new method by considering the nonlinear differential equation. Frame the convex homotopy of the momentum equation to solve the problem by the homotopy perturbation method.

Applying HPM to equation (18) and the momentum equation becomes, we obtain

$$H(u_0, p) = (1 - p)L(u_0) + p\left(L(u_0) + \left(-\epsilon\theta_0 + \frac{1}{2}(\epsilon\theta_0)^2\right)u_0'' + \left(-\epsilon\theta_0' + \epsilon^2\theta_0\theta_0'\right)u_0' + \frac{-\epsilon\theta_0 + \frac{1}{2}(\epsilon\theta_0)^2}{Da}u_0\right), \quad (24)$$

where L is a linear operator and

$$L(u_0) = (1 + \beta i\omega)u_0'' + Su_0' - \left(\frac{1}{Da} + Ha + Rei\omega\right)u_0 + \lambda + Gr\theta_0 + Gc\phi_0. \quad (25)$$

Substituting $L(u_0)$ into equation (24),

$$H(u_0, p) = (1 + \beta i\omega)u_0'' + Su_0' - \left(\frac{1}{Da} + Ha + Rei\omega\right)u_0 + \lambda + Gr\theta_0 + Gc\phi_0 +$$
$$+ p\left(\left(-\epsilon\theta_0 + \frac{1}{2}(\epsilon\theta_0)^2\right)u_0'' + \left(-\epsilon\theta_0' + \epsilon^2\theta_0\theta_0'\right)u_0' + \frac{-\epsilon\theta_0 + \frac{1}{2}(\epsilon\theta_0)^2}{Da}u_0\right). \quad (26)$$

Assuming that

$$u_0 = u_{00} + pu_{01} + p^2 u_{02} + \ldots \quad \text{where } p \to 1. \tag{27}$$

Applying (27) into (26), we formulate the following equation,

$$
\begin{aligned}
H(u_0, p) = {} & (1 + \beta i\omega)\left(u_{00}'' + pu_{01}'' + p^2 u_{02}'' + \ldots\right) + S\left(u_{00}' + pu_{01}' + p^2 u_{02}' + \ldots\right) - \\
& - \left(\frac{1}{Da} + Ha + Rei\omega\right)\left(u_{00} + pu_{01} + p^2 u_{02} + \ldots\right) + \lambda + Gr\theta_0 + Gc\phi_0 + \\
& + p\Bigg(\left(-\epsilon\theta_0 + \frac{1}{2}(\epsilon\theta_0)^2\right)\left(u_{00}'' + pu_{01}'' + p^2 u_{02}'' + \ldots\right) + \\
& + \left(-\epsilon\theta_0' + \epsilon^2\theta_0\theta_0'\right)\left(u_{00}' + pu_{01}' + p^2 u_{02}' + \ldots\right) + \\
& + \frac{-\epsilon\theta_0 + \frac{1}{2}(\epsilon\theta_0)^2}{Da}\left(u_{00} + pu_{01} + p^2 u_{02} + \ldots\right)\Bigg). \tag{28}
\end{aligned}
$$

Comparing the coefficients of p^0, p^1, p^2

$$p^0: \quad (1 + \beta i\omega)u_{00}'' + S u_{00}' - \left(\frac{1}{Da} + Ha + Rei\omega\right)u_{00} + \lambda + Gr\theta_0 + Gc\phi_0. \tag{29}$$

The boundary conditions are given by:

$$
\begin{aligned}
u_{00} = 0 \quad \text{on } y = h_1, \\
u_{00} = 0 \quad \text{on } y = h_2,
\end{aligned} \tag{30}
$$

$$p^1: \quad (1 + \beta i\omega)u_{01}'' + S u_{01}' - \left(\frac{1}{Da} + Ha + Rei\omega\right)u_{01} +$$

$$+ \left(\left(-\epsilon\theta_0 + \frac{1}{2}(\epsilon\theta_0)^2\right)u_{00}'' + \left(-\epsilon\theta_0' + \epsilon^2\theta_0\theta_0'\right)u_{00}' + \frac{-\epsilon\theta_0 + \frac{1}{2}(\epsilon\theta_0)^2}{Da}u_{00}\right). \tag{31}$$

The boundary conditions are as follows

$$
\begin{aligned}
u_{01} = 0 \quad \text{on } y = h_1, \\
u_{01} = 0 \quad \text{on } y = h_2,
\end{aligned} \tag{32}
$$

$$p^2: \quad (1 + \beta i\omega)u_{02}'' + S u_{02}' - \left(\frac{1}{Da} + Ha + Rei\omega\right)u_{02} +$$

$$+ \left(\left(-\epsilon\theta_0 + \frac{1}{2}(\epsilon\theta_0)^2\right)u_{01}'' + \left(-\epsilon\theta_0' + \epsilon^2\theta_0\theta_0'\right)u_{01}' + \frac{-\epsilon\theta_0 + \frac{1}{2}(\epsilon\theta_0)^2}{Da}u_{01}\right). \tag{33}$$

The boundary conditions are

$$
\begin{aligned}
u_{02} = 0 \quad \text{on } y = h_1, \\
u_{02} = 0 \quad \text{on } y = h_2.
\end{aligned} \tag{34}
$$

The formula for u_{02} is quite lengthy. So the following are the approximate solutions for equations (29) and (31) subject to the boundary conditions (30) and (32).

$$u_{00} = A_2 e^{m_5 y} + B_2 e^{m_6 y} + \frac{\lambda}{Z} - e^{m_1 y} J_9 - e^{m_2 y} J_{10} - e^{m_3 y} J_{11} - e^{m_4 y} J_{12},$$

$$u_{01} = A_3 e^{m_7 y} + B_3 e^{m_8 y} + J_{14} + \epsilon \left(A_0 e^{m_1 y} + B_0 e^{m_2 y} \right) \left(J_{18} e^{m_5 y} + J_{19} e^{m_6 y} + J_{13} \right) -$$
$$- \frac{\epsilon^2}{2} \left(\left(A_0 e^{m_1 y} \right)^2 + 2 A_0 B_0 e^{(m_1 + m_2) y} + \left(B_0 e^{m_2 y} \right)^2 \right) \left(J_{18} e^{m_5 y} + J_{19} e^{m_6 y} + J_{13} \right) +$$
$$+ \epsilon \left(J_{16} e^{m_5 y} + J_{17} e^{m_6 y} + J_{15} \right) \left(J_{20} e^{m_1 y} + J_{21} e^{m_2 y} \right) -$$
$$- \epsilon^2 \left(J_{16} e^{m_5 y} + J_{17} e^{m_6 y} + J_{15} \right) \left(A_0 e^{m_1 y} + B_0 e^{m_2 y} \right) \left(J_{20} e^{m_1 y} + J_{21} e^{m_2 y} \right) -$$
$$- \epsilon \left(A_0 e^{m_1 y} + B_0 e^{m_2 y} \right) \left(A_2 e^{m_5 y} + B_2 e^{m_6 y} + \frac{\lambda}{Z} + J_{14} \right) +$$
$$+ \frac{\epsilon^2}{2 Da} \left(\left(A_0 e^{m_1 y} \right)^2 + 2 A_0 B_0 e^{(m_1 + m_2) y} + \left(B_0 e^{m_2 y} \right)^2 \right) \left(A_2 e^{m_5 y} + B_2 e^{m_6 y} + \frac{\lambda}{Z} + J_{14} \right),$$

$$u(y, t) = \left(A_2 e^{m_5 y} + B_2 e^{m_6 y} + \frac{\lambda}{Z} - J_9 - J_{10} - J_{11} - J_{12} + A_3 e^{m_7 y} + B_3 e^{m_8 y} + J_{14} + \right.$$
$$+ \epsilon \left(A_0 e^{m_1 y} + B_0 e^{m_2 y} \right) \left(J_{18} e^{m_5 y} + J_{19} e^{m_6 y} + J_{13} \right) -$$
$$- \frac{\epsilon^2}{2} \left(\left(A_0 e^{m_1 y} \right)^2 + 2 A_0 B_0 e^{(m_1 + m_2) y} + \left(B_0 e^{m_2 y} \right)^2 \right) \left(J_{18} e^{m_5 y} + J_{19} e^{m_6 y} + J_{13} \right) +$$
$$+ \epsilon \left(J_{16} e^{m_5 y} + J_{17} e^{m_6 y} + J_{15} \right) \left(J_{20} e^{m_1 y} + J_{21} e^{m_2 y} \right) -$$
$$- \epsilon^2 \left(J_{16} e^{m_5 y} + J_{17} e^{m_6 y} + J_{15} \right) \left(A_0 e^{m_1 y} + B_0 e^{m_2 y} \right) \left(J_{20} e^{m_1 y} + J_{21} e^{m_2 y} \right) -$$
$$- \epsilon \left(A_0 e^{m_1 y} + B_0 e^{m_2 y} \right) \left(A_2 e^{m_5 y} + B_2 e^{m_6 y} + \frac{\lambda}{Z} + J_{14} \right) +$$
$$\left. + \frac{\epsilon^2}{2 Da} \left(\left(A_0 e^{m_1 y} \right)^2 + 2 A_0 B_0 e^{(m_1 + m_2) y} + \left(B_0 e^{m_2 y} \right)^2 \right) \left(A_2 e^{m_5 y} + B_2 e^{m_6 y} + \frac{\lambda}{Z} + J_{14} \right) \right) e^{i \omega t}. \quad (35)$$

The exact solutions for equations (19) and (20) under the given boundary conditions (21)–(22) are as follows:

$$\theta(y, t) = \left(A_0 e^{m_1 y} + B_0 e^{m_2 y} \right) e^{i \omega t}, \quad (36)$$

$$\phi(y, t) = \left(A_1 e^{m_3 y} + B_1 e^{m_4 y} \right) e^{i \omega t}. \quad (37)$$

The formulas for the rate of velocity, heat transfer and mass transfer are

$$S_f = \beta \left(\frac{\partial u}{\partial y} \right)_{y = h_1, h_2}, \quad (38)$$

$$Nu = - \left(\frac{\partial \theta}{\partial y} \right)_{y = h_1, h_2}, \quad (39)$$

$$Sh = - \left(\frac{\partial \phi}{\partial y} \right)_{y = h_1, h_2}. \quad (40)$$

4. Results and discussion

The influence of the time-dependent viscosity and viscoelasticity on the magnetohydrodynamic oscillatory flow of second-order fluid through thermally radiating wavy walls is investigated. The effect of several physical parameters, such as the Lorentz force Ha, viscoelasticity β, Darcy flow

parameter Da, Peclet number Pe, Schmidt number Sc, and chemical reaction parameter Kr, are investigated on the momentum, energy and concentration profiles of the viscoelastic fluid. By using the slope linear regression method, the rate of skin friction coefficient, heat transfer and velocity are computed and compared for different values of variable viscosity and thermal radiation parameters. $\epsilon = 0.04$, $Pe = 10$ (non-Newtonian fluid), $Q = 1$, $Kr = 1$, $Sc = 1$, $\lambda = 10$, $\beta = 1$, $Gr = 1$, $Gc = 1$, $S = 1$, $Re = 1$, $Da = 1$, $Ha = 1$, $t = 0.1$, $\omega = \frac{\pi}{4}$, $N = 1$ are taken into account in all graph computations.

4.1. Influence of different physical parameters on velocity profiles

Figure 2, a illustrates the velocity profile for different values of viscoelasticity. As the viscoelastic parameter increases, the horizontal velocity of the fluid decreases. Figure 2, b shows the case of variable viscosity, i. e., $\epsilon = 0.04$. Instead of the velocity profiles decreasing with a rise in the values of the viscoelasticity β, the velocity profiles tend to rise. An increase in the viscoelasticity β produces resistance in the fluid flow. An increase in viscoelasticity β implies a decrease in the yield stress of the viscoelastic fluid and a rise in the value of viscoelasticity, this effect creates resistance in the fluid flow. A decrease in fluid velocity is observed to be overpowered by a high amount of temperature, which is injected due to $\epsilon = 0.04$. Hence, the viscoelastic fluid velocity profiles increase.

Viscoelastic fluids exhibit both viscous (flow-like) and elastic (solid-like) behavior. The viscoelastic parameter β usually represents the elasticity or solid-like behavior in the fluid. When viscoelasticity is small ($\beta \leqslant 1$), it implies that the fluid has a predominantly viscous response, meaning it flows more easily than it deforms like a solid. In practical situations, having a small β in non-Newtonian flow cases can simplify mathematical models and calculations. This essentially suggests that the response of fluid to stress is more fluid-like than solid-like, making predictions and analyses easier to handle.
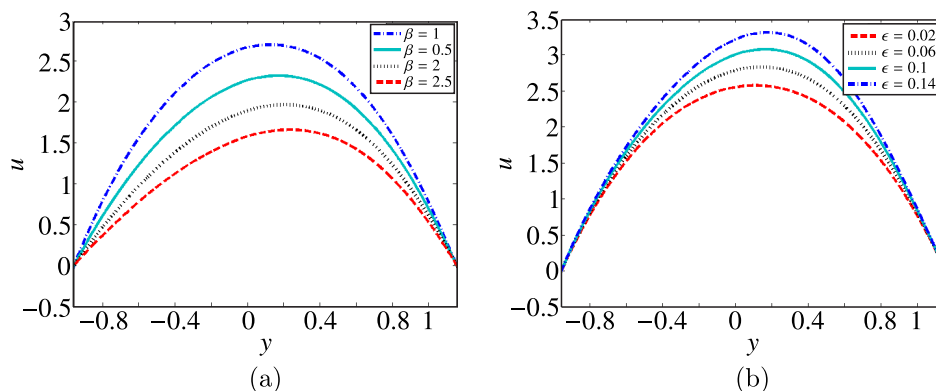

Figure 2. Velocity profile (u) for various values of (a) viscoelasticity and (b) variable viscosity at $Pe = 10$, $Q = 1$, $Kr = 1$, $Sc = 1$, $\lambda = 10$, $Gr = 1$, $Gc = 1$, $S = 1$, $Re = 1$, $Da = 1$, $Ha = 1$, $t = 0.1$, $\omega = \frac{\pi}{4}$, $N = 1$

In Figure 3, a the velocity of the fluid rises as the porous medium permeability varies, which shows the effect of the Darcy number on u. According to the physical theory, as Da increases, the number of physical impediments in the flow channel decreases, enabling the fluid to move more freely and at a faster rate. An electrically conducting viscoelastic fluid subjected to a magnetic field generates a drag-like force known as the Lorentz force. This is due to the interaction of a magnetic field with electrically charged fluid particles, which increases flow resistance and reduces the flow velocity. Within the boundary, this force reduces the fluid velocity. In the absence of a magnetic field, the fluid flow tends to have higher velocities. Hence, the velocity profile decreases as Ha increases, as shown in Figure 3, b, which illustrates the Lorentz force's flow retarding impact. The change in velocity profiles according to oscillation frequency is seen in Figure 4. The velocity profile decreases as the parameter specified above is increased.
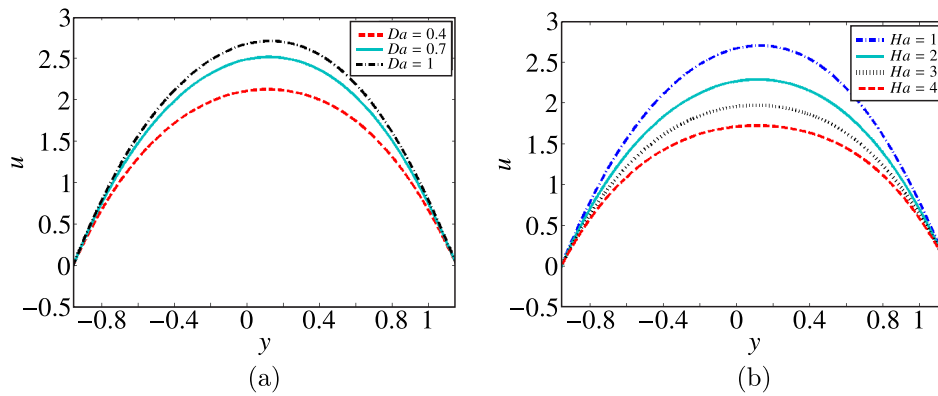
Figure 3. Velocity profile (u) for various values of (a) Darcy number and (b) Hartmann number at $Pe = 10$, $Q = 1$, $Kr = 1$, $Sc = 1$, $\lambda = 10$, $Gr = 1$, $Gc = 1$, $S = 1$, $Re = 1$, $\epsilon = 0.04$, $\beta = 1$, $t = 0.1$, $\omega = \frac{\pi}{4}$, $N = 1$
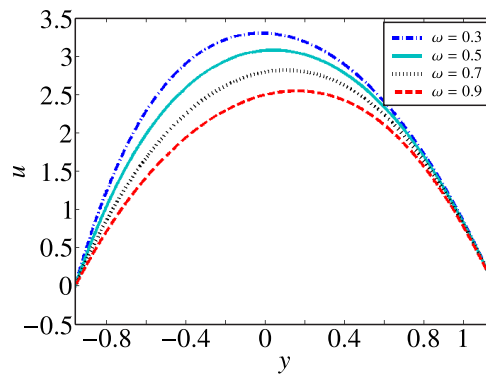

Figure 4. Velocity profile (u) for various values of frequency oscillation parameter at $Pe = 10$, $Q = 1$, $Kr = 1$, $Sc = 1$, $\lambda = 10$, $Gr = 1$, $Gc = 1$, $S = 1$, $Re = 1$, $\epsilon = 0.04$, $\beta = 1$, $Da = 1$, $Ha = 1$, $t = 0.1$, $N = 1$

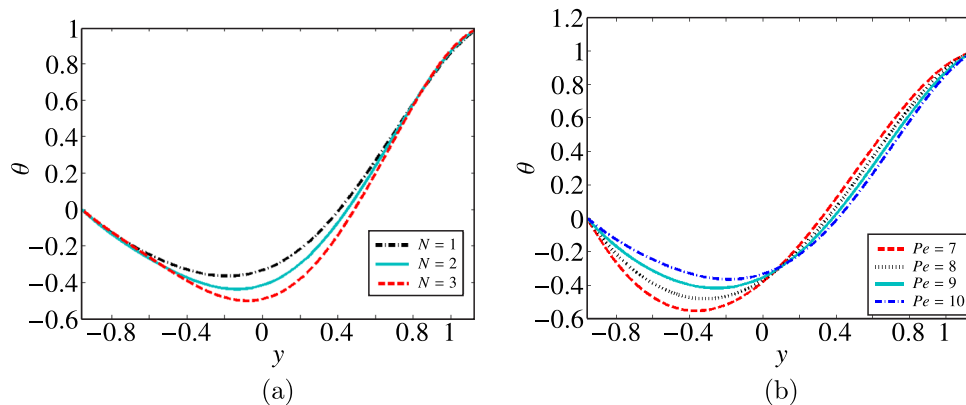

Figure 5. Temperature profile (θ) for various values of (a) thermal radiation parameter and (b) Peclet number at $Q = 1$, $S = 1$, $t = 0.1$, $\omega = \frac{\pi}{4}$

4.2. Influence of different physical parameters on temperature profiles

Figure 5, a demonstrates how the fluid temperature exhibits a descending trend as the radiation parameter increases. It depends on how a heated medium wall surface behaves because the fluid absorbs its own radiation. The flow with a higher Peclet number indicates that the heat transfer by convection is dominant over conduction heat transfer. It gives the relation between conduction and convection

heat transfer. Figure 5, *b* shows the effect of high Peclet numbers on the temperature profile. The fluid temperature increases towards the center of the channel. After that, the opposite effect occurs as higher Peclet numbers indicate that convective heat transfer dominates over conductive heat transfer. For a Peclet number of $Pe \geqslant 7$, it generally indicates that advection is dominant over diffusion. Specifically, in non-Newtonian fluid flow, it implies that the fluid is transported primarily by the flow itself rather than by molecular distribution. This is relevant in situations where convective transport dominates.

4.3. Influence of different physical parameters on concentration profiles

Figure 6, *a* indicates that increasing the chemical reaction parameter progressively reduces the concentration profile. The fundamental reason is that, as the chemical reaction parameter increases, the number of molecules undergoing the chemical reaction increases, resulting in a drop in the concentration field. The Schmidt number is the ratio of the shear component for diffusivity to the diffusivity for mass transfer. Figure 6, *b* anticipates that an increase in Schmidt number corresponds to a weaker fluid diffusivity, allowing a shallow molecular effect to penetrate. As a consequence, the fluid concentration decreases as Sc increases. A smaller value of Sc, means better diffusion of species in fluid concentration. Hence, for a small Schmidt number ($Sc \leqslant 1$) the species concentration in the fluid is higher and vice-versa for both Newtonian and non-Newtonian fluids.

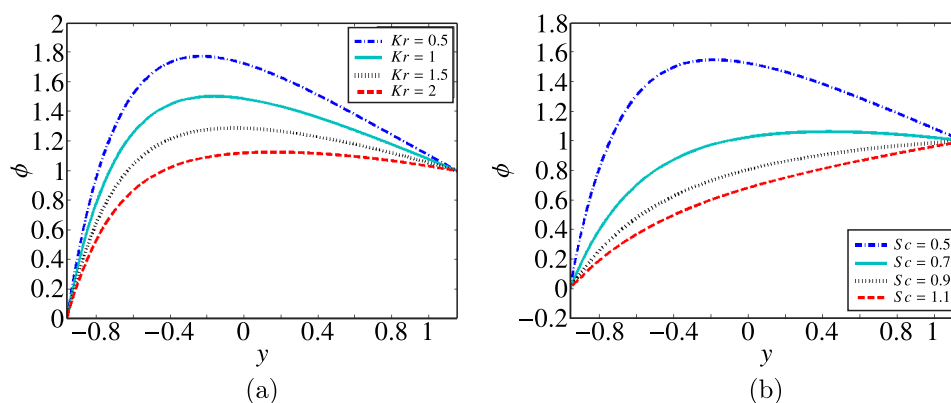Figure 6. Concentration profile (ϕ) for various values of (a) chemical reaction parameter and (b) Schmidt number at $S = 1$, $t = 0.1$, $\omega = \frac{\pi}{4}$

4.4. Skin friction coefficient, Mass transfer rate and Heat transfer rate

Figure 7, *a*, *b* deals with the skin friction coefficient (Sf) for varying values of viscoelasticity β at $y = h_1$ and $y = h_2$. Due to asymmetric wave motion, Sf varies periodically. At the wall $y = = h_1$, Sf initially increases and then decreases for different values of β and vice versa for $y = h_2$. The influence of variable viscosity on the Sf is depicted in Figure 8, *a*, *b*. At both the walls $y = h_1$ and $y = h_2$, Sf initially increases and decreases for various values of ϵ due to asymmetric wave motion and the fluid is dominated by temperature-dependent viscosity.

Figure 9, *a*, *b* displays heat transfer rate for different values of thermal radiation parameter. Due to the wavy walls, the Nusselt number Nu occurs periodically on both walls. Similarly in the case of mass transfer rate for different values of Kr, the Sherwood number Sh occurs periodically.

4.5. Comparative study of heat transfer rate, skin friction coefficient and velocity profile

The rate of increase/decrease in skin friction coefficient Sf and velocity is analyzed using the slope linear regression approach and compared to the given data points. As suggested by [Animasaun
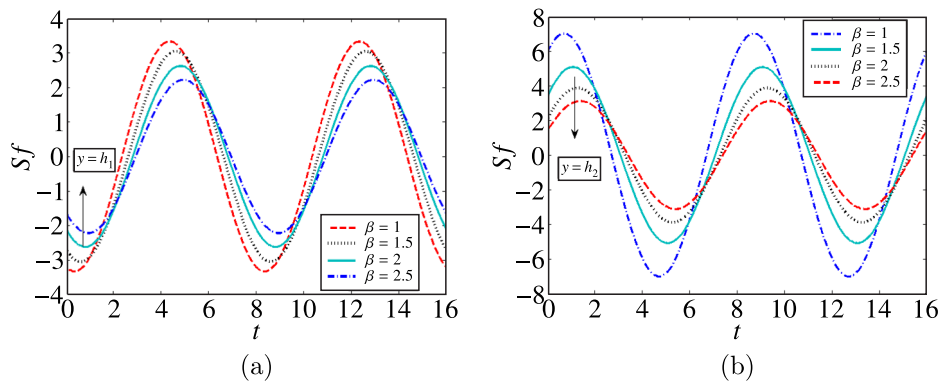
Figure 7. Skin friction coefficient (Sf) for various values of (a) viscoelasticity at $y = h_1$ (right wall) and (b) viscoelasticity at $y = h_2$ (left wall) at $Pe = 10$, $Q = 1$, $Kr = 1$, $Sc = 1$, $\lambda = 10$, $Gr = 1$, $Gc = 1$, $\epsilon = 0.04$, $S = 1$, $Re = 1$, $Da = 1$, $Ha = 1$, $\omega = \frac{\pi}{4}$, $N = 1$
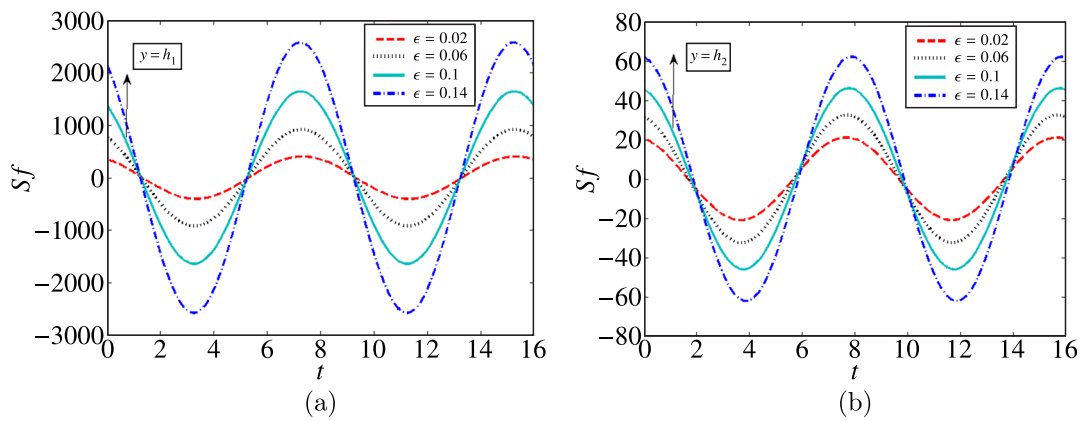
Figure 8. Skin friction coefficient (Sf) for various values of (a) variable viscosity at $y = h_1$ (right wall) and (b) variable viscosity at $y = h_2$ (left wall) at $Pe = 10$, $Q = 1$, $Kr = 1$, $Sc = 1$, $\lambda = 10$, $Gr = 1$, $Gc = 1$, $\beta = 1$, $S = 1$, $Re = 1$, $Da = 1$, $Ha = 1$, $\omega = \frac{\pi}{4}$, $N = 1$

Figure 9. Heat transfer rate (Nu) for various values of (a) thermal radiation parameter at $y = h_1$ (right wall) and (b) thermal radiation parameter at $y = h_2$ (left wall) at $Q = 1$, $S = 1$, $\omega = \frac{\pi}{4}$, $Pe = 10$

et al., 2019] and [Vaidehi, Sasikumar, 2023a], the resulting data are scrutinized here by linear slope regression analysis S_{lp} and are shown in Tables 1 to 4.

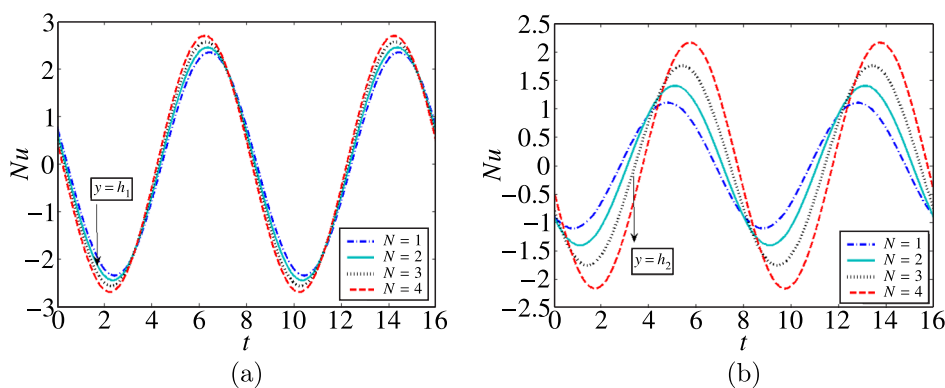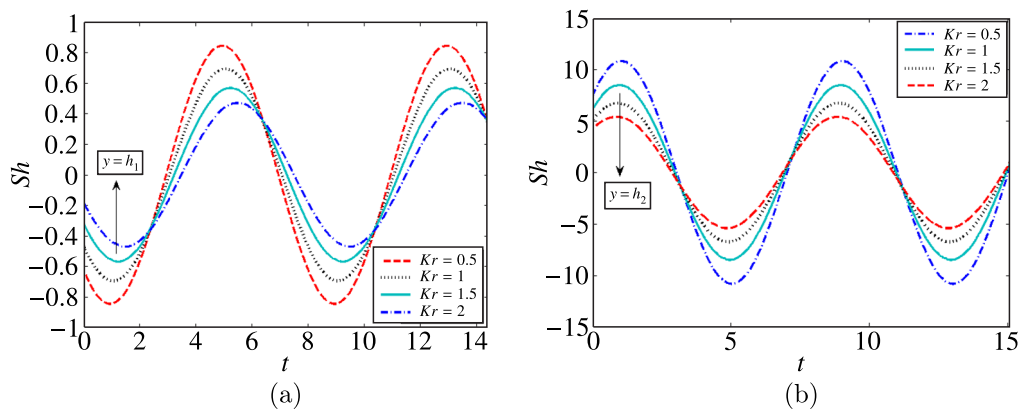Figure 10. Mass transfer rate (Sh) for various values of (a) chemical reaction parameter at $y = h_1$ (right wall) and (b) chemical reaction parameter at $y = h_2$ (left wall) at $S = 1$, $\omega = \frac{\pi}{4}$, $Sc = 1$

1) The rate of increase in the thermal radiation parameter at $N = [0.5, 2]$ and is calculated by S_{lp}. Based on the observations from Table 1, it has been noted that at the thermal radiation parameter ($N = 0.5$), the Sf of the viscoelastic fluid rises over the channel at a rate of -4.417633333. When the thermal radiation parameter ($N = 2$), it has been noted that the Sf of the viscoelastic fluid rises over the channel at a rate of -4.44517619.

Table 1. The Skin friction coefficient of the viscoelastic fluid under the influence of the thermal radiation parameter

S. No.	Skin friction coefficient (Sf)			
y	$N = 0.5$	$N = 1$	$N = 1.5$	$N = 2$
-0.75	4.5417	4.5948	4.6654	4.7555
-0.50	2.8811	2.9044	2.9384	2.9853
-0.25	1.5362	1.5310	1.5290	1.5311
0	0.4528	0.4364	0.4196	0.4024
0.25	-0.5176	-0.5354	-0.5540	-0.5735
0.50	-1.5587	-1.5799	-1.6030	-1.6280
0.75	-2.6353	-2.6340	-2.6337	-2.6346
1	-3.3059	-3.2282	-3.1503	-3.0725
S_{lp}	-4.417633333	-4.41702381	-4.425714286	-4.44517619

2) The rate of decrease in the viscoelasticity at $\beta = [1, 4]$ is tabulated in Table 2. It has been observed that, in the case of viscoelastic parameter $\beta = 1$, the skin friction coefficient of the viscoelastic fluid decreases across the channel at a rate of -4.41702381. When the viscoelastic parameter $\beta = 4$, the skin friction coefficient of the viscoelastic fluid decreases across the channel at a rate of -1.933728571. While comparing the S_{lp} values from Table 1 and Table 2, for higher values of viscoelasticity ($\beta > 1$), the rate of change in the skin friction coefficient of the viscoelastic fluid shows high variations, where the rate of change in Sf at thermal radiation parameter N is relatively stable.

3) The rate of increase in the viscosity variation parameter at $\epsilon = [0, 0.2]$ is tabulated in the Table 3. It has been observed that in the absence of viscosity variation parameter $\epsilon = 0$, the Sf of the viscoelastic fluid rises over the channel at a rate of -3.731904762. When the viscosity variation parameter $\epsilon = 0.2$, the Sf of the viscoelastic fluid rises over the channel at a rate

Table 2. The Skin friction coefficient for various values of viscoelastcity β

S. No.	Skin friction coefficient (Sf)			
y	$\beta = 1$	$\beta = 2$	$\beta = 3$	$\beta = 4$
-0.75	4.5948	3.0929	2.1067	1.5151
-0.50	2.9044	2.2920	1.6934	1.2732
-0.25	1.5310	1.4288	1.1595	0.9201
0	0.4364	0.5707	0.5444	0.4716
0.25	-0.5354	-0.2691	-0.1199	-0.0500
0.50	-1.5799	-1.1618	-0.8454	-0.6404
0.75	-2.6340	-2.1043	-1.6142	-1.2689
1	-3.2282	-2.7542	-2.1744	-1.7270
S_{lp}	-4.41702381	-3.405847619	-2.532604762	-1.933728571

Table 3. The Skin friction coefficient for various values of viscosity variation parameter ϵ

S. No.	Skin friction coefficient (Sf)		
y	$\epsilon = 0$	$\epsilon = 0.1$	$\epsilon = 0.2$
-0.75	4.2136	5.2037	6.3174
-0.50	2.6530	3.2326	3.6489
-0.25	1.4359	1.5472	1.6368
0	0.3449	0.4488	0.4633
0.25	-0.4363	-0.6674	-0.8435
0.50	-1.3275	-1.9817	-2.7133
0.75	-2.3499	-2.8726	-2.8968
1	-2.1127	-2.3600	-1.19754
S_{lp}	-3.731904762	-4.532133333	-4.7471380954

Table 4. The velocity for different values of the viscosity variation parameter under the influence of Lorentz force

S. No.	Velocity					
	($\epsilon = 0$)			($\epsilon = 0.4$)		
y	$Ha = 0.3$	$Ha = 0.6$	$Ha = 0.9$	$Ha = 0.3$	$Ha = 0.6$	$Ha = 0.9$
-0.75	1.0541	1.0115	0.9755	1.1053	1.0591	1.0191
-0.50	1.9522	1.8615	1.7846	2.0709	1.9718	1.8857
-0.25	2.5026	2.3737	2.2645	2.7090	2.5640	2.4381
0	2.7491	2.5976	2.4694	3.0441	2.8672	2.7139
0.25	2.7167	2.5623	2.4318	3.0640	2.8782	2.7174
0.50	2.4060	2.2705	2.1558	2.7300	2.5661	2.4241
0.75	1.7895	1.6942	1.6128	1.9977	1.8867	1.7900
1	0.8136	0.7747	0.7410	0.8624	0.8218	0.7860
S_{lp}	-0.1342476	-0.1351904	-0.1363904	-0.0944476	-0.098538	-0.1023190

of -4.747138095. When comparing the rate of Sf between $\epsilon = 0$ and $\epsilon = 0.2$, the percentage increase is estimated to be 21.3862186%.

4) Table 4 displays that the velocity of the viscoelastic fluid declines in the absence ($\epsilon = 0$) as well as in the presence of the viscosity variation parameter ($\epsilon = 0.4$) of viscoelastic fluid when Ha fluctuates across $[0.3, 0.9]$. The linear slope regression S_{lp} method is used to determine the rate of reduction in the Hartmann number, which varies across the range $Ha = [0.3, 0.9]$. The influence of the Lorentz force ($Ha = 0.3$) on the velocity decreases across the domain at

a rate of -0.1342476 in the absence of the viscosity variation parameter ($\epsilon = 0$), and at a rate of -0.0944476 in the presence of the viscosity variation parameter ($\epsilon = 0.4$). When comparing the velocity rate between case A and case B, the percentage increase is estimated to be $29.6467103\,\%$ for $Ha = 0.3$ and $24.9807996\,\%$ for $Ha = 0.9$.

5) The rate of increase in the thermal radiation parameter at $N = [1, 4]$ is calculated by the linear slope regression S_{lp}. It can be seen from Table 5 that in the case of thermal radiation parameter ($N = 1$), the heat transfer rate of the viscoelastic fluid rises across the channel at a rate of -1.320852381. When the thermal radiation parameter ($N = 4$), the heat transfer rate of the viscoelastic fluid increases across the channel at a rate of -1.722033333.

Table 5. The rate of heat transfer for various values of the thermal radiation parameter N

S. No.	Heat transfer rate (Nu)			
y	$N = 1$	$N = 2$	$N = 3$	$N = 4$
-0.75	0.6453	0.7090	0.7008	0.8876
-0.50	0.4134	0.5269	0.6501	0.7798
-0.25	0.1081	0.2196	0.3861	0.6231
0	-0.3561	-0.3706	-0.4286	-0.4598
0.25	-0.9208	-0.9971	-1.0442	-1.0467
0.50	-1.4065	-1.5599	-1.7146	-1.8639
0.75	-1.5670	-1.6989	-1.8469	-1.9110
1	-1.1729	-1.1702	-1.1808	-1.2068
S_{lp}	-1.320852381	-1.4404	-1.551138095	-1.722033333

4.6. Validation of results

The results of the approximate and numerical solutions are validated and compared in this part. The results are validated with the referenced work produced by [Venkateswarlu et al., 2019] in Table 6. The ordinary differential equations are solved using HPM (semi-analytical method) and numerically using bvp4c solver. Table 6 provides the numerical values of the Nusselt number (Nu) corresponding to different values of Q. It emphasizes a significant rise in the magnitude of Nusselt number, and the resulting values are approximately in agreement with the values presented in the reference table.

Table 6. The effect of heat source parameter Q on the heat transfer rate

S. No.	Nusselt Number (Nu)	
Q	[Venkateswarlu et al., 2019]	Present Study (HPM)
0.1	1.315587	1.2894
0.3	1.898342	1.78674
0.5	2.563548	2.4342
0.7	3.408621	3.3397

As shown in Table 7, the results for both cases indicate minor differences between approximate and numerical solutions. For varying values of the Darcy number, it has been seen that in both solutions the magnitude of "Skin friction coefficient" of the second-order fluid rises.

5. Concluding remarks

The investigation on the influence of variable viscosity and viscoelasticity on the magnetohydrodynamic (MHD) oscillatory flow of a second-order fluid through thermally radiating wavy walls has led to several key findings. The unsteady two-dimensional heat and mass transfer

Table 7. Comparison of the approximate solution and the numerical solution for the skin friction coefficient

S. No.	Skin friction coefficient ($S f$)	
Da	HPM	Bvp4c solution
1	−3.4780	−3.4745
1.5	−3.7001	−3.7006
2	−3.8113	−3.8121
2.5	−3.8755	−3.8774

model has been formulated, and both nonsimilarity and numerical solutions have been adopted to analyze the system. The findings obtained from this study provide valuable insights into the behavior of the fluid flow and guide the investigation.

1. It is worth remarking that the rate of increase/decrease in the skin friction coefficient at viscoelasticity of the second order fluid shows high variations, where the rate of change in $S f$ at the thermal radiation parameter N is relatively stable.

2. The importance of considering the viscosity variation parameter and its interaction with the Lorentz force in determining the velocity behavior of the viscoelastic fluid is highlighted. The percentage increase in velocity demonstrates a significant influence of these factors on the fluid flow characteristics.

3. The decrease in fluid velocity is overpowered by a significant increase in temperature caused by temperature-dependent viscosity. As a result, the velocity profiles of the viscoelastic fluid experience an overall increase.

4. As the Peclet number varies, the fluid temperature increases from the left wall to the center of the channel. The opposite effect is observed towards the right wall, where convective heat transfer exceeds conductive heat transfer.

5. The relationship between Schmidt number ($S c$) and fluid diffusivity has been explored, revealing that a rise in $S c$ corresponds to a weaker fluid diffusivity in the concentration profile.

6. The periodic variations of skin friction coefficient, Nusselt number and Sherwood number are observed due to the asymmetric wavy motion for different values of viscoelasticity, temperature-dependent viscosity, thermal radiation parameter and chemical reaction parameter.

Nomenclature

u — velocity, $\left[\text{ms}^{-1}\right]$;
P — fluid pressure, $\left[\text{kgm}^{-1}\text{s}^{-2}\right]$;
x, y — spatial coordinates, [m];
T_0, T_1 — reference fluid temperatures, [K];
C_0, C_1 — reference fluid concentration, [M];
a_1, b_1 — amplitudes of the wavy walls, [m];
H_1, H_2 — walls of the channel, [m];
h_1, h_2 — nondimensional channel walls;
p — nondimensional fluid pressure;
B_0 — magnetic field intensity, $\left[\text{m}^{-1}\text{A}\right]$;
K — thermal conductivity of the fluid, $\left[\text{Wm}^{-1}\text{K}^{-1}\right]$;
$d_1 + d_2$ — thickness of the channel, [m];

C_p — specific heat at constant pressure, $\left[\text{Jkg}^{-1}\text{K}^{-1}\right]$;

Gr — Grashof number;

Nu — Nusselt number;

T — fluid temperature, [K];

t — time, [s];

g — acceleration due to gravity, $\left[\text{ms}^{-2}\right]$;

d — mean half thickness of the channel, [m];

Ha — Hartmann number;

S — suction/injection parameter;

Pe — Peclet number;

Da — Darcy number;

S_f — skin friction coefficient;

Sh — Sherwood number;

Sc — Schmidt number;

C — concentration of fluid, [M];

Kr — chemical reaction parameter, $\left[\text{Mol l}^{-1}\text{s}^{-1}\right]$;

Q — heat source parameter, [J];

Re — Reynolds number;

D — diffusivity, $\left[\text{m}^2\text{s}^{-1}\right]$;

Gc — modified Grashof number;

N — thermal radiation parameter;

a, b — amplitude ratios;

k^* — porous permeability, $\left[\text{m}^2\right]$.

Greek symbols

v_0 — constant horizontal velocity, $\left[\text{ms}^{-1}\right]$;

λ' — wavelength, [M];

ϵ — viscosity variation parameter;

ω — frequency of oscillation, $\left[\text{s}^{-1}\right]$;

β — viscoelastic fluid parameter;

α — mean radiation absorption coefficient, $\left[\text{Wm}^{-1}\right]$;

θ — dimensionless temperature;

λ — dimensionless pressure gradient;

σ — fluid conductivity, $\left[\text{S m}^{-1}\right]$;

ψ — phase angle, degrees;

β_T — thermal expansion coefficient, $\left[\text{K}^{-1}\right]$;

α_s — stagnation speed, $\left[\text{ms}^{-1}\right]$;

β_C — mass expansion coefficient;

$\mu(T)$ — temperature-dependent viscosity;

ρ — density of fluid, $\left[\text{kg m}^{-3}\right]$;

$\mu(\theta)$ — dimensionless temperature-dependent viscosity;

μ — viscosity of fluid, $\left[\text{N s m}^{-2}\right]$.

Appendix

$$m_1 = \frac{-S + \sqrt{S^2 - 4(N+Q-Pei\omega)}}{2};$$

$$m_2 = \frac{-S - \sqrt{S^2 - 4(N+Q-Pei\omega)}}{2};$$

$$R = \frac{S}{Sc};$$

$$F = \frac{Kr+i\omega}{Sc};$$

$$m_3 = \frac{-R + \sqrt{R^2 + 4F}}{2};$$

$$m_4 = \frac{-R - \sqrt{R^2 + 4F}}{2};$$

$$E = 1 + \beta i\omega;$$

$$Z = Re\,i\omega + Ha + \frac{1}{Da};$$

$$m_5 = \frac{-S + \sqrt{S^2 + 4EZ}}{2E};$$

$$m_6 = \frac{-S - \sqrt{S^2 + 4EZ}}{2E};$$

$$m_7 = \frac{-S + \sqrt{S^2 + 4EZ}}{2E};$$

$$m_8 = \frac{-S - \sqrt{S^2 + 4EZ}}{2E};$$

$$A_0 = \frac{-e^{(m_2-m_1)h_2}}{e^{m_2 h_1} - e^{(m_2-m_1)h_2 + m_1 h_1}};$$

$$B_0 = \frac{1}{e^{m_2 h_1} - e^{(m_2-m_1)h_2 + m_1 h_1}};$$

$$A_1 = \frac{-e^{(m_4-m_3)h_2}}{e^{m_4 h_1} - e^{(m_4-m_3)h_2 + m_3 h_1}};$$

$$B_1 = \frac{1}{e^{m_4 h_1} - e^{(m_4-m_3)h_2 + m_3 h_1}};$$

$$J_1 = \frac{GrA_0 e^{m_1 h_1}}{Em_1^2 + Sm_1 - Z};$$

$$J_2 = \frac{GrB_0 e^{m_2 h_1}}{Em_2^2 + Sm_2 - Z};$$

$$J_3 = \frac{GcA_1 e^{m_3 h_1}}{Em_3^2 + Sm_3 - Z};$$

$$J_4 = \frac{GcB_1 e^{m_4 h_1}}{Em_4^2 + Sm_4 - Z};$$

$$J_5 = \frac{GrA_0 e^{m_1 h_2}}{Em_1^2 + Sm_1 - Z};$$

$$J_6 = \frac{GrB_0 e^{m_2 h_2}}{Em_2^2 + Sm_2 - Z};$$

$$J_7 = \frac{GcA_1 e^{m_3 h_2}}{Em_3^2 + Sm_3 - Z};$$

$$J_8 = \frac{GcB_1 e^{m_4 h_2}}{Em_4^2 + Sm_4 - Z};$$

$$L_1 = \frac{\lambda}{Z} - J_1 - J_2 - J_3 - J_4;$$

$$L_2 = \frac{\lambda}{Z} - J_5 - J_6 - J_7 - J_8;$$

$$A_2 = -\frac{e^{m_6 h_1}}{e^{m_5 h_1}} \cdot \frac{e^{m_5 h_1}(L_2) - e^{m_5 h_2}(L_1)}{e^{m_6 h_1 + m_5 h_2} - e^{m_6 h_2 + m_5 h_1}} - \frac{L_1}{e^{m_5 h_1}};$$

$$B_2 = \frac{e^{m_5 h_1}(L_2) - e^{m_5 h_2}(L_1)}{e^{m_6 h_1 + m_5 h_2} - e^{m_6 h_2 + m_5 h_1}};$$

$$J_9 = \frac{GrA_0}{Em_1^2 + Sm_1 - Z};$$

$$J_{10} = \frac{GrB_0}{Em_2^2 + Sm_2 - Z};$$

$$J_{11} = \frac{GcA_1}{Em_3^2 + Sm_3 - Z};$$

$$J_{12} = \frac{GcB_1}{Em_4^2 + Sm_4 - Z};$$

$$J_{13} = -m_1^2 J_9 - m_2^2 J_{10} - m_3^2 J_{11} - m_4^2 J_{12};$$

$$J_{14} = -J_9 - J_{10} - J_{11} - J_{12};$$

$$J_{15} = -m_1 J_9 - m_2 J_{10} - m_3 J_{11} - m_4 J_{12};$$

$$J_{16} = m_5 A_2;$$

$$J_{17} = m_6 B_2;$$

$$J_{18} = m_5^2 A_2;$$

$$J_{19} = m_6^2 B_2;$$

$$J_{20} = m_1 A_0;$$

$$J_{21} = m_2 B_0;$$

$$J_{22} = \left(A_0 e^{m_1 h_1} + B_0 e^{m_2 h_1}\right)\left(J_{18} e^{m_5 h_1} + J_{19} e^{m_6 h_1} + J_{13}\right);$$

$$J_{23} = \left(\left(A_0 e^{m_1 h_1}\right)^2 + 2 A_0 B_0 e^{(m_1+m_2) h_1} + \left(B_0 e^{m_2 h_1}\right)^2\right)\left(J_{18} e^{m_5 h_1} + J_{19} e^{m_6 h_1} + J_{13}\right);$$

$$J_{24} = \left(J_{16} e^{m_5 h_1} + J_{17} e^{m_6 h_1} + J_{15}\right)\left(J_{20} e^{m_1 h_1} + J_{21} e^{m_2 h_1}\right);$$

$$J_{25} = \left(J_{16} e^{m_5 h_1} + J_{17} e^{m_6 h_1} + J_{15}\right)\left(A_0 e^{m_1 h_1} + B_0 e^{m_2 h_1}\right)\left(J_{20} e^{m_1 h_1} + J_{21} e^{m_2 h_1}\right);$$

$$J_{26} = \left(A_0 e^{m_1 h_1} + B_0 e^{m_2 y h_1}\right)\left(A_2 e^{m_5 h_1} + B_2 e^{m_6 h_1} + \frac{\lambda}{Z} + J_{14}\right);$$

$$J_{27} = \left(\left(A_0 e^{m_1 h_1}\right)^2 + 2 A_0 B_0 e^{(m_1+m_2) h_1} + \left(B_0 e^{m_2 h_1}\right)^2\right)\left(A_2 e^{m_5 h_1} + B_2 e^{m_6 h_1} + \frac{\lambda}{Z} + J_{14}\right);$$

$$J_{28} = \left(A_0 e^{m_1 h_2} + B_0 e^{m_2 h_2}\right)\left(J_{18} e^{m_5 h_2} + J_{19} e^{m_6 h_2} + J_{13}\right);$$

$$J_{29} = \left(\left(A_0 e^{m_1 h_2}\right)^2 + 2 A_0 B_0 e^{(m_1+m_2) h_2} + \left(B_0 e^{m_2 h_2}\right)^2\right)\left(J_{18} e^{m_5 h_2} + J_{19} e^{m_6 h_2} + J_{13}\right);$$

$$J_{30} = \left(J_{16} e^{m_5 h_2} + J_{17} e^{m_6 h_2} + J_{15}\right)\left(J_{20} e^{m_1 h_2} + J_{21} e^{m_2 h_2}\right);$$

$$J_{31} = \left(J_{16} e^{m_5 h_2} + J_{17} e^{m_6 h_2} + J_{15}\right)\left(A_0 e^{m_1 h_2} + B_0 e^{m_2 h_2}\right)\left(J_{20} e^{m_1 h_2} + J_{21} e^{m_2 h_2}\right);$$

$$J_{32} = \left(A_0 e^{m_1 h_2} + B_0 e^{m_2 y h_2}\right)\left(A_2 e^{m_5 h_2} + B_2 e^{m_6 h_2} + \frac{\lambda}{Z} + J_{14}\right);$$

$$J_{33} = \left(\left(A_0 e^{m_1 h_2}\right)^2 + 2 A_0 B_0 e^{(m_1+m_2) h_2} + \left(B_0 e^{m_2 h_2}\right)^2\right)\left(A_2 e^{m_5 h_2} + B_2 e^{m_6 h_2} + \frac{\lambda}{Z} + J_{14}\right);$$

$$L_3 = J_{14} + \epsilon J_{22} - \frac{\epsilon^2}{2} J_{23} + \epsilon J_{24} - \epsilon^2 J_{25} - \epsilon J_{26} + \frac{\epsilon^2}{2Da} J_{27};$$

$$L_4 = J_{14} + \epsilon J_{28} - \frac{\epsilon^2}{2} J_{29} + \epsilon J_{30} - \epsilon^2 J_{31} - \epsilon J_{32} + \frac{\epsilon^2}{2Da} J_{33};$$

$$A_3 = -\frac{e^{m_8 h_1}}{e^{m_7 h_1}} \cdot \frac{e^{m_7 h_1}(L_4) - e^{m_7 h_2}(L_3)}{e^{m_8 h_1 + m_7 h_2} - e^{m_8 h_2 + m_7 h_1}} - \frac{L_3}{e^{m_7 h_1}};$$

$$B_3 = \frac{e^{m_7 h_1}(L_4) - e^{m_7 h_2}(L_3)}{e^{m_8 h_1 + m_7 h_2} - e^{m_8 h_2 + m_7 h_1}}.$$

Acknowledgment

Declaration of competing interest

The authors of this article declare that they have no competing interest to disclose.

References

Abbas Z., Rafiq S., Sheikh M., Aly S. Oscillatory Darcy flow of non-Newtonian Casson fluid with temperature-dependent viscosity in a porous channel // Arabian Journal for Science and Engineering. — 2020. — Vol. 45, No. 9. — P. 7247–7255.

Ali M. E. The effect of variable viscosity on mixed convection heat transfer along a vertical moving surface'// International Journal of Thermal Sciences. — 2006. — Vol. 45, No. 1. — P. 60–69.

Al-Khafajy D. G. Effects of heat transfer on MHD oscillatory flow of Jeffrey fluid with variable viscosity through porous medium // Advances in Applied Science Research. — 2016. — Vol. 7, No. 3. — P. 179–186.

Al-Khafajy D. G. S. Radiation and mass transfer effects on MHD oscillatory flow for Jeffery fluid with variable viscosity through porous channel in the presence of chemical reaction // Sci. Int. — 2019. — P. 27–28.

Animasaun I. L. Casson fluid flow with variable viscosity and thermal conductivity along exponentially stretching sheet embedded in a thermally stratified medium with exponentially heat generation // Journal of Heat and Mass Transfer Research. — 2015a. — Vol. 2, No. 2. — P. 63–78.

Animasaun I. L. Effects of thermophoresis, variable viscosity and thermal conductivity on free convective heat and mass transfer of non-darcian MHD dissipative Casson fluid flow with suction and nth order of chemical reaction // Journal of the Nigerian Mathematical Society. — 2015b. — Vol. 34, No. 1. — P. 11–31.

Animasaun I. L., Ibraheem R. O., Mahanthesh B., Babatunde H. A. A meta-analysis on the effects of haphazard motion of tiny/nano-sized particles on the dynamics and other physical properties of some fluids // Chinese Journal of Physics. — 2019. — Vol. 60. — P. 676–687.

Astanina M. S., Sheremet M. A. Simulation of mixed convection of a variable viscosity fluid in a partially porous horizontal channel with a heat-generating source // Computer research and modelling. — 2019. — Vol. 11, No. 1. — P. 95–107.

Baag S., Mishra S. R., Dash G. C., Acharya M. R., Panda S. Exact solution for MHD elastico-viscous flow in porous medium with radiative heat transfer // Pramana. — 2022. — Vol. 96, No. 4. — P. 178.

Barkilean J., Jagadeesan S. Heat transfer characteristics on MHD oscillatory radiative nanofluid with $H_2O/C_2H_6O_2$ (basefluid): a comparative study of different nanoparticles of various shapes // International Journal of Heat and Technology. — 2023. — Vol. 41, No. 3.

Bataller R. C. Viscoelastic fluid flow and heat transfer over a stretching sheet under the effects of a nonuniform heat source, viscous dissipation and thermal radiation // International Journal of Heat and Mass Transfer. — 2007. — Vol. 50, No. 15–16. — P. 3152–3162.

Falade J. A., Ukaegbu J. C., Egere A. C., Adesanya S. O. MHD oscillatory flow through a porous channel saturated with porous medium // Alexandria engineering journal. — 2017. — Vol. 56, No. 1. — P. 147–152.

Jiang X., Zhang H., Wang S. Unsteady magnetohydrodynamic flow of generalized second grade fluid through porous medium with Hall effects on heat and mass transfer // Physics of Fluids. — 2020. — Vol. 32, No. 11. — P. 113105.

Liao S. J. An approximate solution technique not depending on small parameters: a special example // International Journal of Non-Linear Mechanics. — 1995. — Vol. 30, No. 3. — P. 371–380.

Loenko D. S., Sheremet M. A. Numerical modeling of the natural convection of a non-Newtonian fluid in a closed cavity // Computer Research and Modeling. — 2020. — Vol. 12, No. 1. — P. 59–72.

Mahmoud M. A. A. Chemical reaction and variable viscosity effects on flow and mass transfer of a non-Newtonian visco-elastic fluid past a stretching surface embedded in a porous medium // Meccanica. — 2010. — Vol. 45. — P. 835–846.

Mishra S. R., Dash G. C., Acharya M. Mass and heat transfer effect on MHD flow of a visco-elastic fluid through porous medium with oscillatory suction and heat source // International Journal of Heat and Mass Transfer. — 2013. — Vol. 57, No. 2. — P. 433–438.

Mukhopadhyay S., Layek G. C. Effects of thermal radiation and variable fluid viscosity on free convective flow and heat transfer past a porous stretching surface // International Journal of Heat and Mass Transfer. — 2008. — Vol. 51, No. 9–10. — P. 2167–2178.

Ogulu A., Bestman A. R. Deep heat muscle treatment a athematical model-I // Acta Physica Hungarica. — 1993. — Vol. 73. — P. 3–16.

Pearson J. R. A. Variable-viscosity flows in channels with high heat generation // Journal of Fluid Mechanics. — 1977. — Vol. 83, No. 1. — P. 191–206.

Popov V. S., Popova A. A. Modeling of hydroelastic oscillations for a channel wall possessing a nonlinear elastic support // Computer research and modelling. — 2022. — Vol. 14, No. 1. — P. 79–92.

Raju K., Parandhama A., Raju M. C., Ramesh Babu K. Unsteady MHD free convection Jeffery fluid flow of radiating and reacting past a vertical porous plate in Slip-flow regime with heat source // Frontiers in Heat and Mass Transfer (FHMT). — 2018. — Vol. 10.

Raptis A. Radiation and viscoelastic flow // International Communications in Heat and Mass Transfer. — 1999. — Vol. 26, No. 6. — P. 889–895.

Rundora L., Makinde O. D. Effects of suction/injection on unsteady reactive variable viscosity non-Newtonian fluid flow in a channel filled with porous medium and convective boundary conditions // Journal of Petroleum Science and Engineering. — 2013. — Vol. 108. — P. 328–335.

Salem A. M. Variable viscosity and thermal conductivity effects on MHD flow and heat transfer in viscoelastic fluid over a stretching sheet // Physics letters A. — 2007. — Vol. 369, No. 4. — P. 315–322.

Sasikumar J., Bhati D., Bhaskar V. Effect of heat and mass transfer on MHD oscillatory flow through asymmetric wavy channel in a porous medium with suction and injection // AIP Conference Proceedings. — 2020. — Vol. 2277, No. 1.

Sasikumar J., Bhuvaneshwari S., Govindarajan A. Diffusion of chemically reactive species in MHD oscillatory flow with thermal radiation in the presence of constant suction and injection // Journal of Physics: Conference Series. — 2018. — Vol. 1000, No. 1. — P. 012033.

Sasikumar J., Govindarajan A. Effect of heat and mass transfer on MHD oscillatory flow with chemical reaction and slip conditions in asymmetric wavy channel // Journal of Engineering and Applied Sciences. — 2016. — Vol. 11, No. 2. — P. 1164–1170.

Sasikumar J., Harinisha N., Anitha S. MHD oscillatory flow through porous medium in rotating wavy channel with heat source // AIP Conference Proceedings. — 2019. — Vol. 2112, No. 1.

Sasikumar J., Senthamarai T. Chemical reaction and viscous dissipation effect on MHD oscillatory blood flow in tapered asymmetric channel // Mathematical Modeling and Computing. — 2022. — Vol. 9, No. 4. — P. 999–1010.

Selvi R. K., Muthuraj R. MHD oscillatory flow of a Jeffrey fluid in a vertical porous channel with viscous dissipation // Ain Shams Engineering Journal. — 2018. — Vol. 9, No. 4. — P. 2503–2516.

Siva T., Kumbhakar B., Jangili S., Mondal P. K. Unsteady electro-osmotic flow of couple stress fluid in a rotating microchannel: An analytical solution // Physics of Fluids. — 2020. — Vol. 32, No. 10 — P. 102013.

Vaidehi P., Sasikumar J. Darcy flow of unsteady Casson fluid subject to thermal radiation and Lorentz force on wavy walls: case of slip flow for small and large values of plastic dynamic viscosity // Thermal Science and Engineering Progress. — 2023a. — P. 101885.

Vaidehi P., Sasikumar J. Thermo-diffusion and chemical reaction effect on MHD oscillatory flow of viscoelastic fluid in an asymmetric wavy channel under the influence of magnetic field // Journal MESA. — 2023b. — Vol. 14, No. 2. — P. 373–394.

VeeraKrishna M., Subba Reddy G., Chamkha A. J. Hall effects on unsteady MHD oscillatory free convective flow of second grade fluid through porous medium between two vertical plates // Physics of fluids. — 2018. — Vol. 30, No. 2. — P. 023106.

Venkateswarlu B., Bhagya Lakshmi K., Samantha Kumari S., Satya Narayana P. V. Magnetohydrodynamic oscillatory flow of a physiological fluid in an irregular channel // SN Applied Sciences. — 2019. — Vol. 1. — P. 1–13.